JOURNAL OF MATERIALS SCIENCE 26 (1991) 5534–5542

Creep failure mechanisms in a particulate-filled epoxy resin

J. W. SMITH*‡, W. J. CANTWELL*, A DEMARMELS§, H. H. KAUSCH*
* *Laboratoire de Polymères, Ecole Polytechnique Fédérale de Lausanne, CH-1007 Lausanne, Switzerland*
§ *Corporate Research Center, Asea Brown Boveri, CH-8050 Zürich, Switzerland*

The deformation-induced volume damage in a series of creep specimens is examined in this investigation in order to improve the basic understanding of creep failure in particulate-reinforced epoxy resins. The results are correlated with the fracture surface morphology reported elsewhere. Volume damage was found to consist of matrix shear yielding, silica-particle debonding and matrix cracking. Fracture is shown to be initiated by shear yielding and debonding which is followed by sub-critical crack growth, demonstrating the importance of volume damage in fracture. Sub-critical crack growth occurs by debonding or by void coalescence depending on the temperature and loading conditions. The temperature and loading dependence of volume damage and the above crack propagation mechanisms are examined and presented graphically in a damage mechanism map.

1. Introduction

Particulate-filled epoxy resins are used in the electrical power industry in the construction of electrical switching gear where properties such as high electrical resistance, high strength and modulus as well as long life-times under load with a minimum of creep are desirable. Silica-filled epoxy resins have been used for two decades in such applications and have performed well; however, there is an increasing demand for improved performance. For example, although toughened by the addition of silica particles, epoxy resins are brittle materials, an undesirable property for structural applications. Under long-term loading conditions at low and intermediate temperatures, the filled epoxy creeps very little, but it exhibits a time-dependent failure which is difficult to predict. The root of these problems lies in a lack of understanding of the basic deformation and damage mechanisms which lead to failure.

The fracture surface morphology of the particulate-filled epoxies used in this investigation have been investigated in detail by Cantwell and co-workers [1, 2]. In this work the authors observed a number of different regions on the fracture surface which they explained. Essentially, the fracture surface could be divided up into zones as shown in Fig. 1. Fracture was shown to initiate at a defect which might be some foreign object introduced during specimen preparation or an unusually large or poorly bonded particle. This was followed by a zone on the fracture surface in which all or many of the filler particles were debonded from the matrix. It was shown that in this debonded zone (later called the sub-critical zone [2]) the crack propagated sub-critically. The size of this zone varied significantly with temperature and loading conditions. Following the sub-critical zone the fracture surface was first smooth, where the crack was shown to be accelerating, and then rough where the crack had reached its limiting velocity for the material.

Cantwell *et al.* [1] showed that in most cases, fracture in creep was initiated by debonding at some defect. Initiation was followed by sub-critical crack growth which formed a debonded sub-critical zone on the fracture surface. For a given temperature, larger sub-critical zones corresponded to failure at longer times. This is shown in Fig. 2, where the size of the sub-critical zone increases with time to failure. In terms of the static-fatigue life-time of this material, the sub-critical zone is of great importance as its growth will determine the lifetime of structural components manufactured from this material. In a subsequent investigation [2], it was shown that fracture in short-term strength tests was also preceded by sub-critical crack growth (debonding). In the course of these investigations it became evident that specimens with large sub-critical zones exhibited stress-whitening in the volume which was most intense under the sub-critical zone in the region of the fracture origin.

Stress-whitening is due to the scattering of light from free surfaces within the volume of the material. In silica-filled epoxy resins, these scattering centres are debonded particles and microcracks created during deformation [3]. In short-term tensile experiments the volume damage has been correlated with the fracture

‡ *Present address*: Department of Materials Science and Engineering and the Materials Science Center, Cornell University, Ithaca, NY 14853, USA.

0022–2461/91 $03.00 + .12

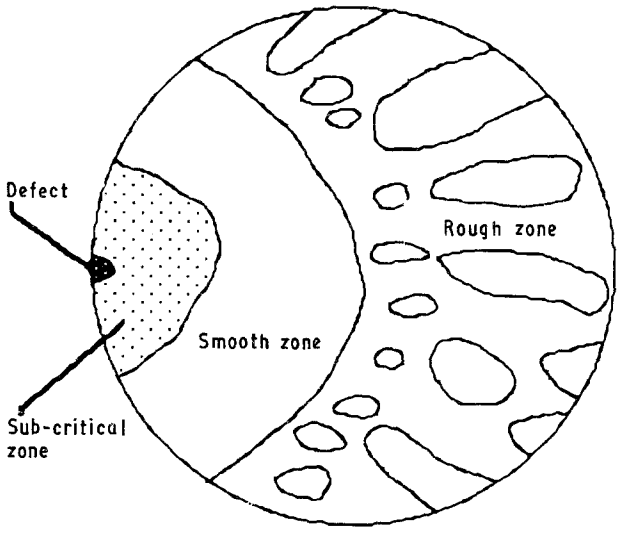

Figure 1 Schematic diagram of a typical fracture surface of a silica-filled epoxy tensile specimen. Fracture may initiate at a defect followed by a sub-critical zone where particles are debonded. The crack accelerates in the smooth zone and reaches limiting velocity in the rough zone.

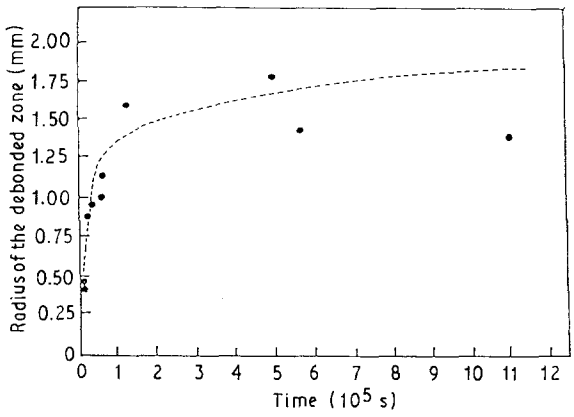

Figure 2 The variation of the size of the sub-critical zone with failure time in the standard silica-filled epoxy at 85 °C [1].

process and three types of crack propagation have been identified [2]. These included rapid brittle fracture, crack propagation by debonding and crack propagation by coalescence of debonding. The occurrence of a particular type of crack propagation is dependent on the rate and temperature of loading.

In this investigation the damage mechanisms in a series of tensile creep specimens are identified and characterized in terms of temperature and load. Because of the lower loads and resulting slower deformation rates, the volume damage and sub-critical cracks develop more slowly and are more numerous. Post-failure analysis often reveals partially propagated cracks adjacent to the critical crack, which allows observation of partially propagated cracks. This allows a more detailed microstructural investigation than was possible with short-term experiments. In the following paragraphs the observed volume damage is correlated with previous fracture surface studies to synthesize the mechanisms of creep failure in silica-filled epoxy resins.

2. Experimental procedure

The material used in this investigation was hydantoin-based epoxy resin cured with an acid anhydride hardener from Ciba Geigy, the details of which are shown in Table I. The liquid resin and hardener were mixed manually at room temperature until the mix was homogeneous. The quartz flour was dried in an oven at 160 °C for at least 16 h immediately prior to casting. The hot flour was then added to the resin and mixed manually and then briefly with an electric mixer until homogeneous. The resulting slurry was then evacuated for 3 min and poured into moulds (preheated to 80 °C) followed by another 4 min under vacuum. The vacuum was then removed and the system was allowed to gel at 80 °C for 4 h followed by a 16 h cure at 160 °C. The resulting material was opaque and brittle with a glass transition of 125 °C. The cast tensile specimens were dumb-bell shaped with a 80 mm gauge length and a 100 mm^2 circular cross-section.

The constant-load creep tests were carried out at temperatures of 23, 50, 85, and 105 °C and at static loads of 20, 40, 60, and 80% of the short-term strength at the given temperature. The tests were conducted in four separate temperature-controlled ovens equipped with a series of rods and levers which multiplied the static loads (lead weights) by a factor of ten. While most specimens loaded to 60 and 80% load failed, many of those at 20 and 40% load had not failed after 2 years and thus tests were stopped. This system is the same as reported previously by Cantwell *et al.* [1].

Microstructural investigations were conducted using optical microscopy and thin sectioning technique described in detail by Smith [4]. Essentially, failed specimens are sectioned parallel to the principal stress adjacent to the fracture origin. The piece containing the fracture origin is then mounted on an optically transparent slide. By first cutting followed by grinding, the section is reduced to a thickness of 50 μm which is then polished and observed in polarized light using a transmitted light microscope.

3. Observations

3.1. Stress-whitening

Stress-whitening in silica-filled epoxy resins is more evident in creep than in the short-term strength tests reported previously [2]. In general it is whiter, and larger volumes of the material are whitened. It is never uniformly distributed throughout the test specimens, due to the fact that it originates preferentially in areas of stress concentration. These include mould parting

TABLE I Material composition

Component	Type	Parts by weight
Hydantoin-based epoxy resin	CY225*	100
	Arcast 350*	100
Anhydride hardener	Hy 925*	160
Quartz flour	W10†	600

* Ciba Geigy, Basel, Switzerland.
† Quartzwerke Frechen, Germany.

lines, corners and changes in cross-section as well as large defects.

In tensile creep, stress-whitening occurs in bands running parallel to the principal stress as shown in Fig. 3a. In specimens with circular cross-sections, these bands initiate at the parting line and grow radially into the volume (Fig. 3b). On occasions, large defects cause the localization of stress-whitening into shear bands originating at the defect [1]. In compressive creep, extensive stress-whitening occurs in the deformation zone. In the absence of inhomogeneities, the whitening in compression is very dense and quite uniform; however, there is ususally a very sharp distinct boundary between the undeformed dead zone and the whitened material in the deformation zone as shown in Fig. 4.

3.2. Time–temperature dependence of damage

Stress-whitening in the silica-filled epoxy is due to particle–matrix debonding and matrix microcracking [3]. This volume damage begins in the vicinity of the outside surface of the tensile specimen, but it develops differently depending on the temperature and to a lesser extent on the creep load. Fig. 5 is a transmitted light micrograph of the damage in a specimen loaded to 60% at 23 °C with a failure time of 22×10^6 s. Five debonding events are evident (dark vertical cracks) and at the right of the picture a fractured particle is clearly visible. The debonded particles are much less obvious; however, they are visible as white areas on either side of the dark lines of debonding. In all cases, the voids have not propagated significantly beyond the interface of the particles and damage is only evident near the outside surface of the specimen.

Fig. 6 shows a typical specimen at 60% load and 85 °C. The number of debonding events is limited and again occurs only near the surface of the specimen. The character of the damage differs from that at lower temperatures in that stable cracks from debonded particles have propagated into the matrix prior to failure. Increasing the temperature or decreasing the

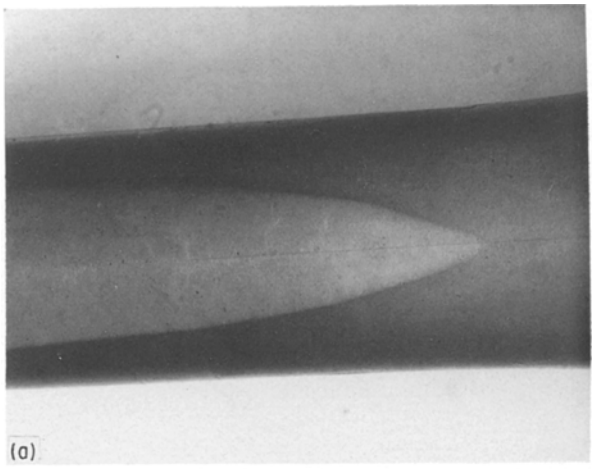

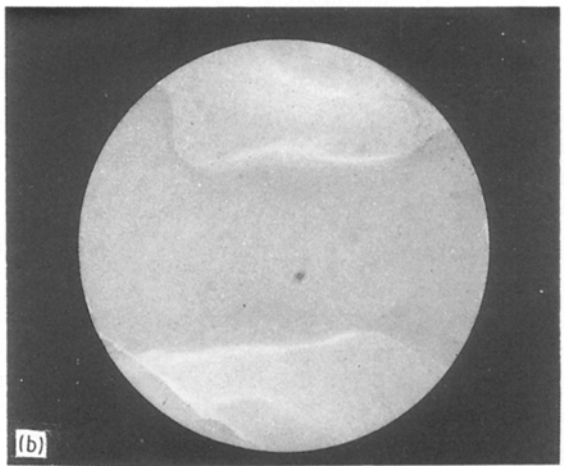

Figure 3 (a) Extensive stress-whitening in the silica-filled epoxy along the mould parting line of a tensile creep specimen tested at 105 °C and 40% load; (b) cross-sectional view of the specimen in (a) showing the radial growth from the parting lines.

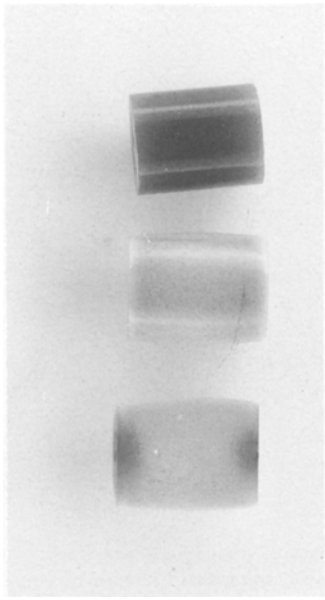

Figure 4 Creep compression specimen showing uniform stress-whitening. Left: undeformed, middle: deformed at 85 °C and 60% load, right: same as middle, sectioned to reveal interior.

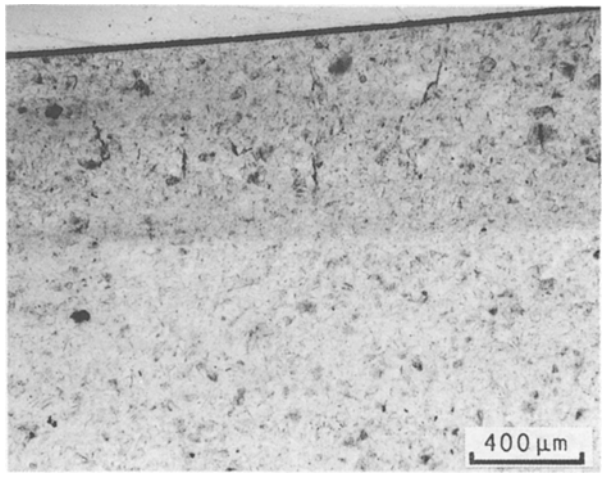

Figure 5 Transmitted bright-field micrograph of a specimen loaded to 60% at 23 °C which failed in 22×10^6 s. Five debonding events are visible as black cracks lying perpendicular to the principal stress. The tensile direction is horizontal.

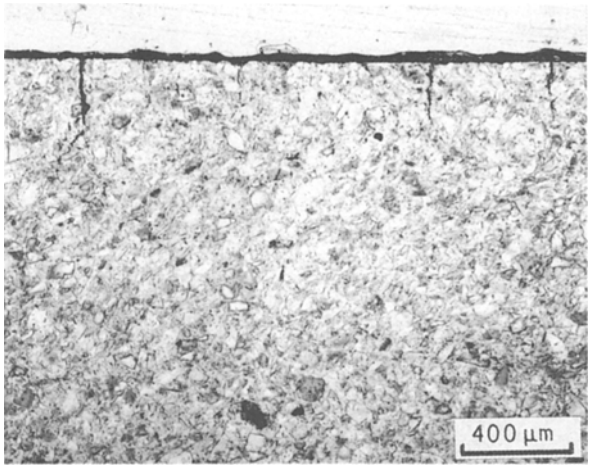

Figure 6 Transmitted bright-field micrograph of specimen fractured at 5.47×10^5 s at 60% and 85 °C.

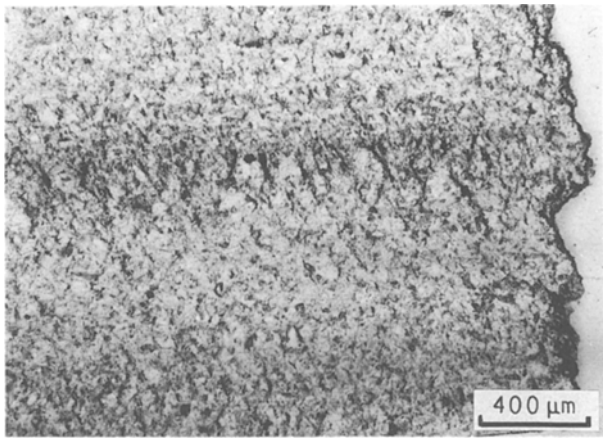

Figure 7 Specimen tested at 105 °C, 40% load and failed at 9.17×10^4 s.

load from this point results in the suppression of these long cracks, an increase in the number of debonded particles and damage penetration further into the interior of the specimen.

Fig. 7 shows an example of a specimen tested at 105 °C and 40% load that failed in 9.17×10^4 s. The damage is extensive and is present throughout the specimen although it is denser in some regions than others. The banded nature of stress-whitening is seen clearly in this picture as the horizontal dark band caused by a network of debonding (compare Fig. 7 with Fig. 3a). It is interesting to note that the long cracks present at 85 °C are no longer present. Instead the material has debonded in many locations rather than propagating a small number of cracks through the matrix. Increasing load at 105 °C results in fracture with less damage accumulation.

In order to quantify the debonding process, the number of voids created by debonded particles in a standard area of 2 mm^2 in the most damaged volume of a number of specimens was counted. The results are plotted in Fig. 8 where the number of debonds is plotted as a function of time. Each point on the plot represents only one sample and therefore the results are not statistically correct; however, certain trends may be identified. Increasing the temperature results in more damage at shorter times and decreasing the stress at a given temperature has the same effect. The temperature–load dependence is indicative of a thermally activated process and is due to the dependence of debonding on shear yielding.

3.3. Time–temperature dependence of shear yielding

Maximum shear yielding in creep occurs at 105 °C. This is to be expected when approaching the glass transition (125 °C), especially at lower loads. Shear yielding is evident both as shear bands and as a general birefringence of the matrix and is of the same character as that observed in strength tests [2, 3]. A typical transmitted polarized light micrograph of shear banding is shown in Fig. 9. The cross-hatched

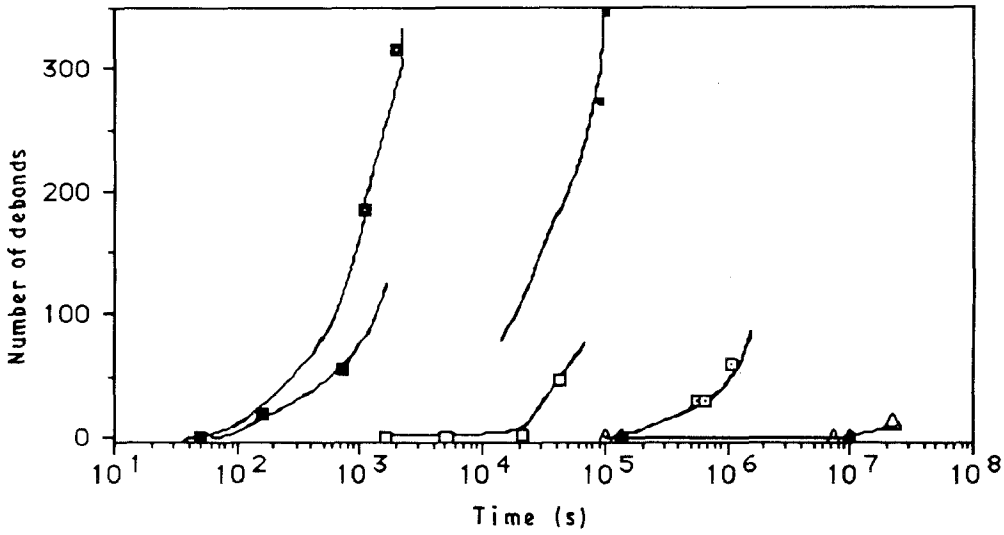

Figure 8 The variation of debonding in the volume as a function of time under load: (△) 23 °C, 60%; (▲) 50 °C, 80%; (□) 85 °C, 80%; (⊡) 85 °C, 60%; (■) 105 °C, 80%; (◘) 105 °C, 60%; (▪) 105 °C, 40%. The number of debonds represents the number of visible debonded voids in a 2 mm^2 area of a thin section taken in the volume of the most extensive whitening. Note that the curves at 105 °C (60 and 80%) are the same within the expected data scatter.

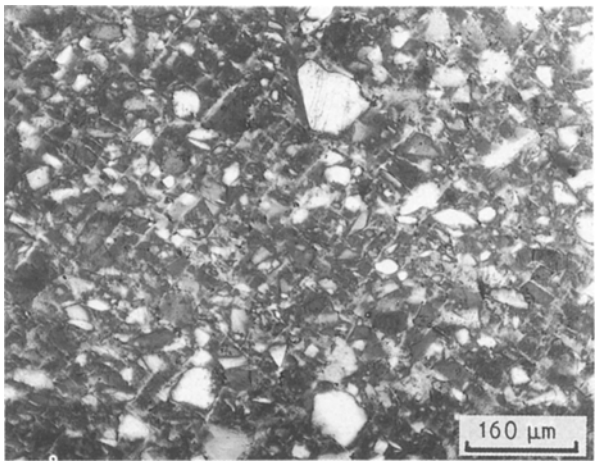

Figure 9 Shear yielding at 105 °C and 60% load. Polarized transmitted light micrograph. Failure time 2×10^3 s.

nature of the shear bands can be seen quite clearly due to their birefringent nature. Fig. 10a and b show shear yielding at 85 °C and 60% load (1.1×10^6 s). The bands are less distinct at low magnification but they are unmistakable at high magnification. Also visible in Fig. 10b is debonding between the poles of two closely spaced particles.

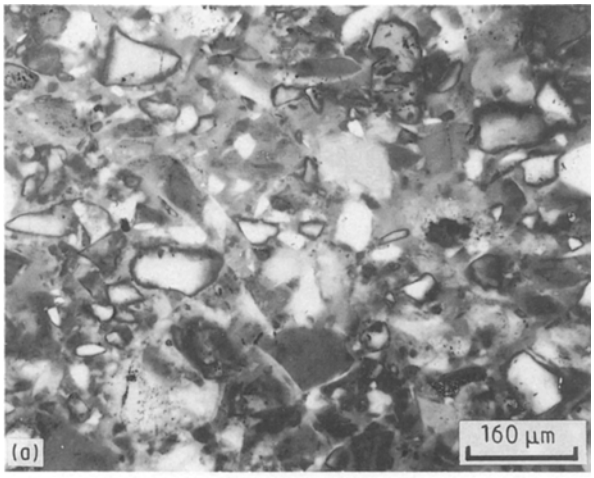

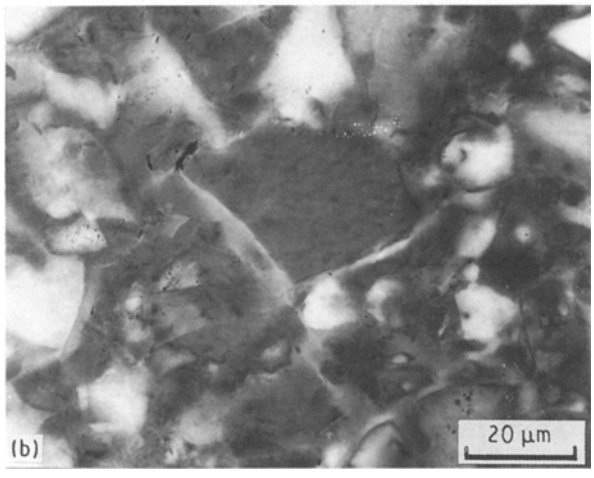

Figure 10 (a) Polarized transmitted light micrograph of a specimen failed in 1.1×10^6 s at 85 °C and 60%. Shear bands are less distinct than in Fig. 9; however, they are unmistakable at higher magnification (b).

Just as damage is not uniform throughout the specimen, neither is shear yielding. Whereas debonding is most prevalent at the surface and in areas of high particle density, shear bands are more visible in the central regions of the specimen and regions of low particle density. This may be due to the fact that where debonding is extensive, there is considerable interference from debonds, cracks and particles which make it difficult to observe the matrix clearly. There is, however, overlap of the two phenomena as shown in Fig. 11.

Once the load is increased to 80%, shear bands are no longer visible at 85 °C. Shear banding was not observed in any creep specimens tested at temperatures below 85 °C. There may have been some residual birefringence around the isolated debonded particles, but it was too ambiguous to be conclusive. While shear bands can be photographed quite easily, the matrix bulk shear yielding is evident as a change in birefringence observed by rotating the microscope stage. This could not be easily reproduced in a photograph. We believe that shear yielding exists at the lower temperature; however, it is limited to such small zones or is so diffuse that it is not evident with the given observation techniques.

3.4. Stress-whitening and the sub-critical zone

In previous investigations [1, 2] the sub-critical zone was identifiable as a region of debonded particles on the fracture surface surrounding the initiation. At low temperatures and especially at high loads, the sub-critical zone was small or negligible in size and thus the debonding was limited to the one or two particles needed to form a critical-sized crack which could accelerate unstably. In these cases, no stress-whitening was visible in the volume. As the temperature was increased and loads were decreased, the sub-critical zone grew in size and volume damage began to become evident.

The fracture surface morphology of the sub-critcal zone also varies with time and temperature. At high temperatures and low loads, the sub-critical zone is

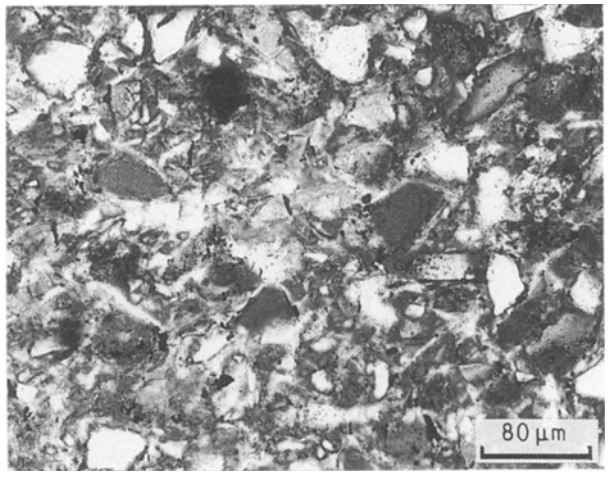

Figure 11 Shear yielding and debonding in a specimen tested at 105 °C and 60% with failure time 2×10^3 s.

usually quite rough whereas at higher loads and lower temperatures the zone is smoother and tends to lie perpendicular to the direction of applied stress. This is shown in Fig. 12 where fracture surface profiles corresponding to the two cases are shown.

The surface of the sub-critical zone is often stress-whitened and large sub-critical zones are usually accompanied by stress-whitening in the underlying volume. Fig. 13 shows a long-term creep specimen tested at 105 °C, 40% load with a failure time of 9.17×10^4 s. The fracture surface has been gold-coated to highlight the sub-critical zone, whereas the circumference is left uncoated to reveal the internal stress-whitening. The exact area of the debonded fracture surface does not correspond to the volume of stress-whitening under the fracture surface and yet the two phenomena would seem to be related. These observations are explained in the following section.

4. Mechanisms of failure in creep

4.1. Fracture initiation

Previous work has shown that the fracture of particulate-filled epoxy composites may be initiated by flaws [1, 5]. Foreign bodies, air bubbles and unusually large filler particles introduced during fabrication are typical examples. Such flaws, if larger than the dimensions of the filler particles, initiate failure. In the absence of such flaws, the presence of filler particles with a distribution of sizes introduces inherent flaws. In either case, the applied stress is amplified by the defect or large particle and shear yielding occurs in the matrix. This is followed by the separation of the flaw–matrix interface, i.e. debonding. It is this coupling of shear yielding and debonding that leads to the time–temperature dependence of damage demonstrated in Fig. 8.

The crack initiation process is shown in Fig. 14 which is taken from the the edge of a specimen deformed at 85 °C and 80% load and a failure time of 4.93×10^4 s. In the lower left corner, a triangular particle has debonded at all three corners and then an interfacial crack has formed along the upper interface.

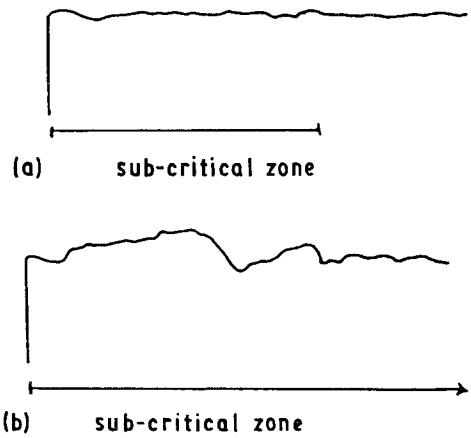

Figure 12 Tracings of the fracture surface topography, illustrating the morphologies of the sub-critical zones for specimens tested at (a) 85 °C and 80% and (b) 105 °C and 50%.

At low temperatures and high loads the mere existence of one such debonded body is sufficient to initiate rapid fracture. This is shown schematically in Fig. 15a. The only damage evident in this case is the single debonding event which initiated the fracture. This debond is often but not always evident on the fracture surface, but no volume damage is evident. Following the initial debonding, the crack accelerates rapidly, propagating predominantly through the matrix as shown in Fig. 15a.

It is this fundamental mechanism which is responsible for the initiation of all tensile failures in this material regardless of the loading conditions. The lifetime of a particular test specimen is thus dependent on two events. The first is the time it takes to generate an interfacial crack. The second is the time it takes this interfacial crack to grow to a critical size capable of propagating unstably. The length of these two times is strongly dependent on the time, temperature and loading conditions.

4.2. Sub-critical crack propagation

4.2.1. Crack propagation by debonding

At 85 °C there is sufficient ductility within the matrix such that the presence of a few voids due to particle debonding is not a sufficient condition to initiate fracture. In fact, as seen in previous photos (Fig. 6), it is possible for the material to remain intact in spite of

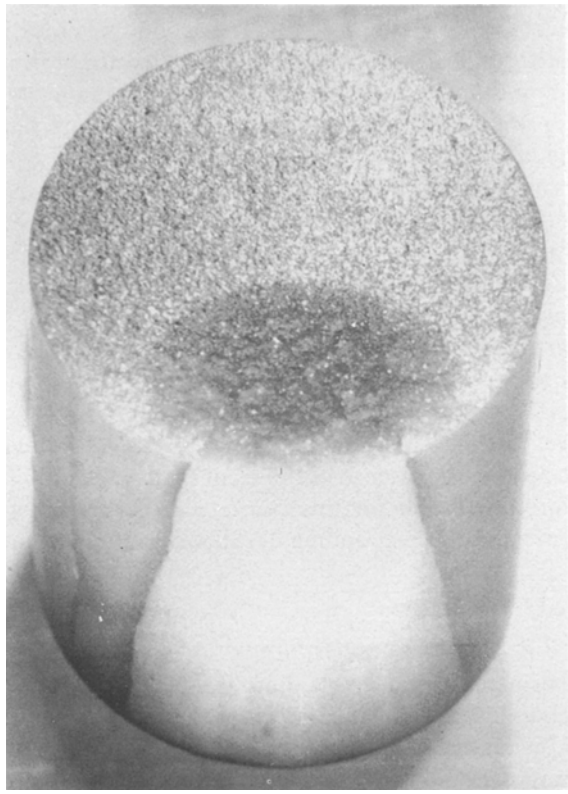

Figure 13 A severely stress-whitened specimen with a large sub-critical zone (105 °C, 40% and $t_f = 9.17 \times 10^4$ s) showing the extension of the latter zone on the fracture surface beyond the underlying debonded volume. The fracture surface is gold-coated to highlight the sub-critical zone.

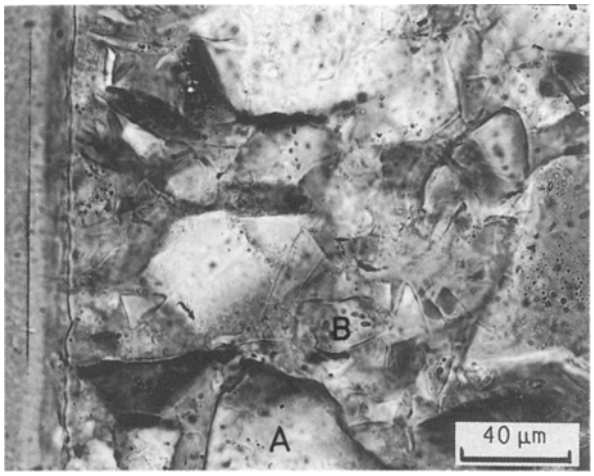

Figure 14 The initiation of a crack by debonding. The triangular particle (lower left) is debonded at both top and bottom. The resulting crack has caused debonding at two particles adjacent to the crack. The tensile direction is vertical and the specimen was loaded at 85 °C and 80%. Failure time 4.3×10^4 s.

the existence of cracks 5 to 10 particle diameters in length.

The initiation of these cracks was illustrated in Fig. 14, where there is a process zone in front of the new interfacial crack which has caused debonding of particles A and B. At lower loads for the same temperature, the same type of crack is able to grow sub-critically as shown in Fig. 16 where the specimen underwent creep at 85 °C and 60% load for 5.47×10^5 s. The cracks initiated in the same way as in Fig. 14 and have progressed from pole to pole. During this time the matrix bridging the debonding crack has failed some distance behind the crack tip, thus forming a continuous crack. This is shown schematically in Fig. 15b. Here a process zone has developed in front of the crack tip. The crack propagation mechanism described above is called "propagation by debonding" and is associated with slow, localized sub-critical crack propagation.

The cracks described above have been observed only near the outer surfaces of the specimens at the parting line where stresses are concentrated. In addition, debonding appears to be concentrated in these crack planes and thus the damage is not spread all over the interior volume. Once a debonding event occurs, in the absence of sufficient matrix ductility it is more favourable for this crack to grow than it is to generate other debonding events on different planes.

4.2.2. Fracture by coalescence of debonding

The increased shear yielding at 105 °C causes more debonding and at the same time reduces the sensitivity of the matrix to the cracks formed by debonding. As a result debonding is more extensive at fracture than at lower temperatures as shown in Fig. 7. In this case the dark vertical lines indicate the large number of debonding events that have occurred. Fig. 17 is a polarized transmitted light micrograph tested at 105 °C at 60% load with a failure time of 2×10^3 s.

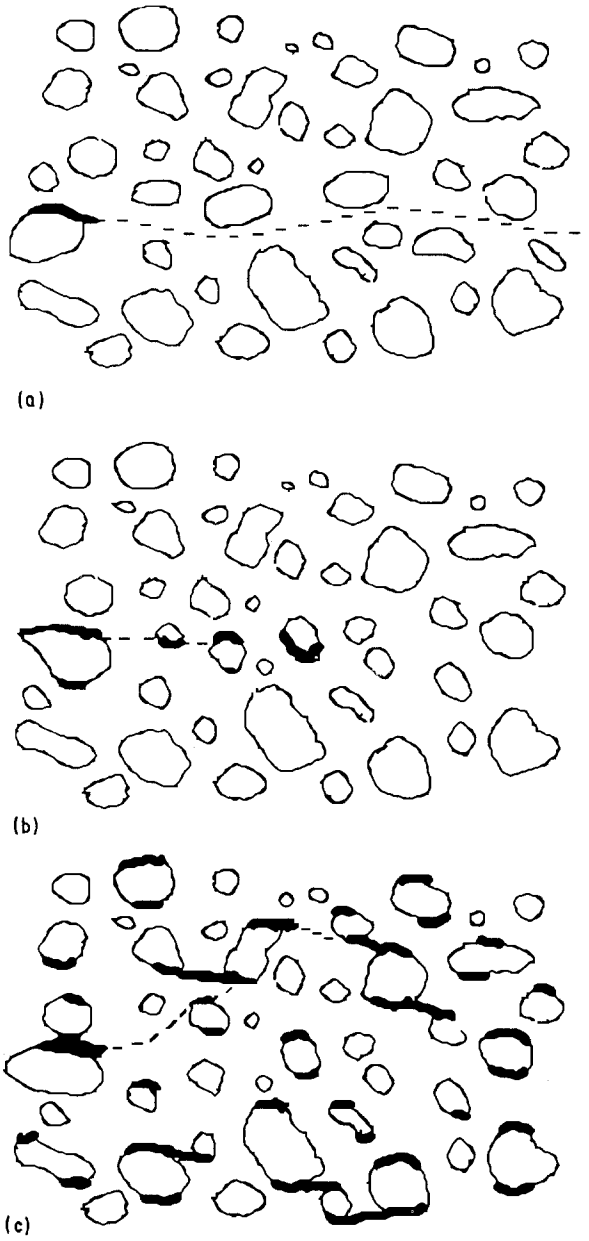

Figure 15 Schematic diagram of crack propagation mechanisms. (a) Rapid brittle fracture: fracture initiated at defect or debonded particle, no volume damage. (b) Crack propagation by debonding: sub-critical zone smooth, limited volume damage (isolated debonding). (c) Crack propagation by void coalescence: sub-critical zone rough, large and three-dimensional, stress-whitening visible due to extensive volume damage (debonding).

Virtually every particle in this micrograph is debonded, resulting in dozens of interfacial cracks. For the most part, however, the matrix has remained intact and thus the load may continue to be supported.

This phenomenon may be explained by the extensive shear yielding that occurs at these temperatures. Fig. 11 is from the same specimen as Fig. 17 but is taken near the centre of the specimen where debonding is less intense. In Fig. 11, shear yielding is quite extensive and has delayed debonded interfacial cracks from propagating into the matrix.

The damage mechanism at 105 °C is one of network debonding and is controlled by shear yielding. Eventually, the integrity of the material is damaged so severely by debonding that it can no longer support

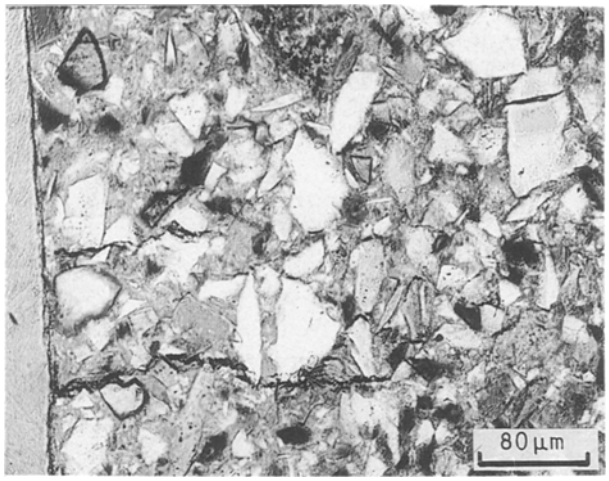

Figure 16 Crack propagation by debonding in a specimen tested at 85 °C, 80% with time to failure of 5.47×10^5 s.

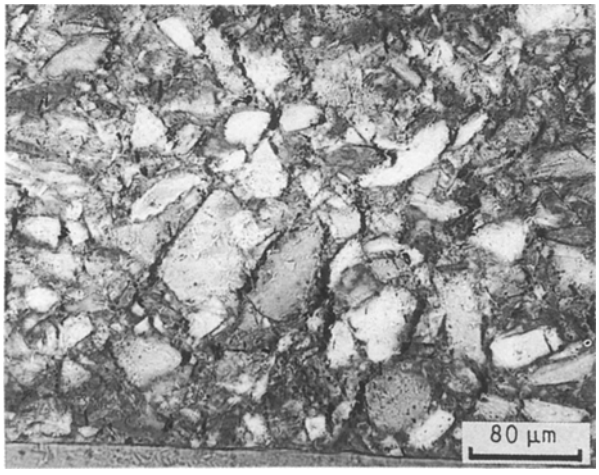

Figure 17 Polarized light micrograph of extensive debonding in a specimen tested at 105 °C, 60% load with a failure time of 2×10^3 s. These debonded voids will link up together to form a crack and eventual fracture.

the load. This is shown schematically in Fig. 15c, where the crack has initiated in the middle of a very large damage zone. The sub-critical crack growth is governed by the already existing damage ahead of it. In this case separate debonded particles are linked up by ductile tearing of the matrix in fracture by void coalescence.

4.3. Volume damage and the sub-critical zone

The crack initiated at 85 °C propagates through undamaged material by debonding particles ahead its tip. The forming crack at 105 °C is different in that it must propagate through already debonded material. Thus, the propagation direction of the higher-temperature crack is governed by the position of already existing voids rather than by creating debonding at the crack tip. While this is again a stable slow-moving crack it does not necessarily propagate on a parallel plane, and thus in the case of highly damaged specimens (long times and low loads) the fracture surface may be quite rough.

This explains the differences in the roughness of the sub-critical zones in Fig. 12. The rough surface was caused by fracture through the coalescence of debonding, with the roughness being due to the crack searching the path of least resistance. The straight surface (Fig. 12a) was due to crack propagation by debonding. In this case the crack propagated straight, driven by the local stress field, and generated its own damage as it propagated.

These two mechanisms also explain why the sub-critical zone on the fracture surface in Fig. 13 extends farther than the underlying stress-whitening. Initially debonding occurred in the volume followed by sub-critical crack growth by void coalescence. Eventually, this sub-critical crack reached the end of the debonded volume; however, it was still not large enough to accelerate. Thus, it continued to propagate sub-critically but this time by debonding until it became unstable and accelerated, resulting in failure. Therefore, the debonded fracture surface outside the stress-whitened volume was due to crack propagation by debonding.

4.4. Damage mechanism map

The temperature–stress dependence of the volume damage is shown more clearly in the damage mechanism map of Fig. 18. The solid circles correspond to broken specimens and the damage observed represents the damage at failure for the given specimen. The unfilled circles represent tests that were interrupted prior to failure, so that the damage observed had not evolved to the point of fracture.

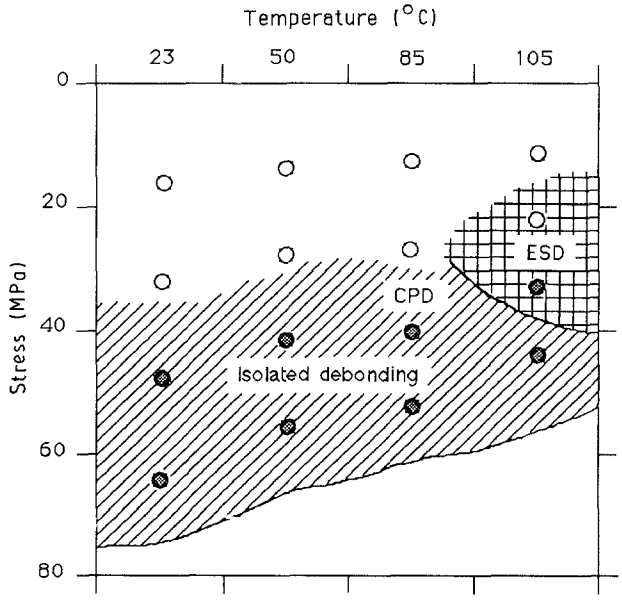

Figure 18 Damage mechanism map showing the stress–temperature dependence of damage in the silica-filled epoxy resin. ESD: extensive shear yielding and debonding. CPD: crack propagation by debonding. (○) Unbroken specimen, (●) broken specimen.

Damage is most prevalent at 105 °C in the cross-hatched region where extensive shear yielding and debonding (ESD) resulted in sub-critical crack growth by void coalescence. In the cross-barred region, fracture was preceded by sub-critical crack growth by debonding. At 60% load, isolated debonding was evident while at the lowest temperatures (80% load) damage was limited to a small debonded sub-critical zone on the fracture surface. The effect of reducing the stress at a given temperature is to reduce the sensitivity of the material to damage, presumably by shear yielding, and thus damage at failure is more extensive at a given temperature for specimens with lower loads. It is self evident that lower stresses exhibit longer failure times.

Unfortunately the damage at failure of the specimens tested at 20 and 40% loads could not be assessed completely as the lower-temperature specimens had not failed after extended times (up to 6×10^7 s) under load, and some specimens at 105 °C were removed prematurely due to failure of the adhesively bonded strain gauges [4]. However, at 105 °C and 40% load, the specimens, although unfractured, were extensively damaged and would eventually have failed by void coalescence. At 23 °C and 60% load, isolated debonding was evident in a specimen which failed after 2.2×10^6 s. It is tempting to suggest that if carried out to completion, the tests at low loads might accumulate more damage than the high-load specimens for an equivalent temperature. Although the above microstructural evidence suggests this is so, it can not be presumed without experimental evidence.

Crack propagation by debonding could be studied easily at the higher temperatures (marked CPD in Fig. 18), as the simultaneous growth of more than one crack meant that partially propagated cracks could be observed. However, the debonding on the fracture surfaces of specimens tested at lower temperatures, and the absence (or limited debonding) of volume damage indicates that these failures were preceded by crack propagation by debonding as well. The difference between "rapid brittle fracture", "crack propagation by debonding" and "fracture by void coalescence" is simply the size of the process zone at the crack tip as shown schematically in Fig. 15. At low temperatures it is very small with limited debonding and shear yielding at the very tip of the crack. Increasing the temperature increases the size of this zone until at high temperatures, it is so large that it ceases to be a crack-tip phenomenon. In this case it is better to think of failure in two steps beginning with bulk deformation damage, followed by initiation and propagation of a crack through damaged material.

5. Summary and conclusions

Combining the fracture surface observations and the volume damage observations enables us to accurately describe the creep failure process in these materials. Fracture is initiated by the debonding of a particle or defect. At low temperatures and high loads, the limited matrix ductility restricts the plastic zone size and rapid brittle fracture ensues. Increasing the temperature and/or decreasing the load allows growth of the plastic zone which begins to encompass additional silica particles in the vicinity of the crack-tip zone. Particles in the crack plane debond and the crack jumps through the matrix extending the crack incrementally, albeit sub-critically, resulting in crack propagation by debonding (this should not be confused with stick–slip fracture as the macroscopic displacement here remains linear). Once the crack reaches a critical size, debonding ceases and rapid acceleration and fracture ensues. In the extreme case of high temperatures and low loads (approaching T_g) the matrix becomes so ductile that shear yielding and debonding are extensive. Sub-critical crack propagation proceeds by coalescence of debonding only after a large volume of the material has been damaged. These mechanisms can be correlated with the temperature and loading conditions and are displayed in the damage mechanism map in Fig. 18.

References

1. W. J. CANTWELL, A. C. ROULIN MOLONEY and T. KAISER, *J. Mater. Sci.* **23** (1988) 1614.
2. W. J. CANTWELL, J. W. SMITH, H. H. KAUSCH and T. KAISER, *ibid.* **24** (1990) 633.
3. J. W. SMITH, T. KAISER, A. C. ROULIN MOLONEY and H. H. KAUSCH, *ibid.* **23** (1989) 3833.
4. J. W. SMITH, in "Fractography and Failure Mechanisms of Polymers and Composites", edited by A. C. Roulin-Moloney (Elsevier Applied Science, London, UK, 1989) Ch. 1.
5. A. C. ROULIN MOLONEY, H. H. KAUSCH, T. KAISER and H. R. BEER, *J. Mater. Sci.* **22** (1987) 381.

Received 1 May
and accepted 30 November 1990